

Final Report
To the NOAA Joint Hurricane Testbed (JHT) Program

Project Title: Improving the Hurricane WRF-Wave-Ocean Coupled System for Transition to Operations

Award Period: 08/01/2007 - 07/31/2009

Principal Investigator: Isaac Ginis
Graduate School of Oceanography
The University of Rhode Island

December, 2009

Executive Summary

The primary goal of this project was to improve the operational hurricane predictive capabilities at the NOAA's Environmental Modeling Center/National Centers for Environmental Prediction by transitioning recent improvements in the air-sea momentum flux parameterizations and the ocean model initialization made by the URI research group into to the Hurricane WRF (HWRF) modeling system. This work was conducted in close collaboration with our EMC colleagues, building directly upon our successful joint EMC/GFDL/URI coupled model research program. We also collaborated with scientists at NOAA/ESRL on the implementation of the NOAA/ESRL sea-spray parameterization scheme into the HWRF model.

The following major tasks were conducted:

- *Implementing and testing the URI wave boundary layer in the HWRF coupled system.*
- *Improving air-sea momentum and heat flux parameterization in the HWRF model by including the effects of wave breaking, sea-spray, and wave-current interaction.*
- *Improving ocean initialization in the HWRF coupled system by implementing new methods for assimilating satellite and in-situ measurements.*

This report summarizes the main work accomplishments and the results.

Tasks completed:

I. Implementing the URI wave boundary layer model into the HWRF

- a) *Improving drag coefficient formulation*

We have implemented an improved drag coefficient parameterization into the operational version of HWRF by upgrading the wave boundary layer (WBL) model of Moon et al. (2007). The WBL model is based on the theoretical model of Moon et al. (2004a-c) and derived from coupled wave-wind (CWW) model simulations of ten tropical cyclones in the Atlantic Ocean during 1998-2003. The upgraded WBL model incorporates the observational results from the CBLAST field experiment (Black et al., 2007) and the estimations of drag coefficient distribution based on GPS sonde wind profiles by Powell (2007). In the improved WBL model, a new formulation for the nondimensional surface roughness (Charnock coefficient) has been derived in order to better match the model results with the observations. Fig. 1 shows C_d vs. wind speed at various sections relative to the storm center. These sections represent composite distributions based on simulations of Hurricanes Noel (2007), Helene and Florence (2006), Katrina, Rita, Emily, Dennis (2005), Ivan and Frances (2004), and Isabel and Fabien (2003). The HRD wind analyses available at every 6 hours were used as the wind input into the model. The new parameterization is now more consistent with the Powell (2007) results but still cannot reproduce the extreme high and low values of C_d in his estimations. We speculate that one possible reason for the observed low values of C_d is related to the sea spray effect, which is not included in this WBL model. Recent studies (e.g., Andreas et al. 2004) suggest that sea sprays may significantly reduce the drag coefficient at very high wind speeds. The sea spray effect is now being implemented in the new coupled wind-wave-current framework as discussed below.

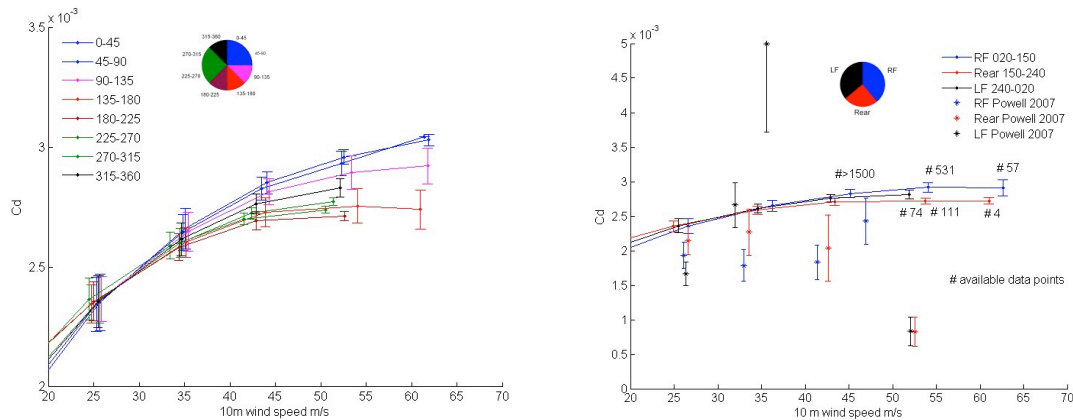


Figure 1. Drag coefficient (C_d) vs. wind speed. Left panel shows C_d in 8 sectors relative to the storm center. Each sector is 45° where the zero degree direction is aligned with the storm movement vector. Right panel shows C_d in 3 sectors with the sizes corresponding to those in Powell (2007). Powell's data are shown for comparison.

The WBL model was recently upgraded further by implementing the coupled wind and wave formulation of Kukulka and Hara (2008a,b) that includes the enhanced form drag of breaking waves. Breaking and non-breaking waves induce air-side fluxes of momentum and energy in a thin layer above the air-sea interface within the constant flux layer (the wave boundary layer). By imposing momentum and energy conservation in the wave boundary layer and wave energy conservation, Kukulka and Hara (2008a,b) have derived coupled nonlinear advance-delay differential equations governing the wind speed, turbulent wind stress, wave height spectrum, and the length distribution of breaking wave

crests. The system of equations is closed by introducing a relation between wave dissipation (due to breaking waves) and the wave height spectrum. Wave dissipation is proportional to nonlinear wave interactions, if the wave curvature spectrum is below the threshold saturation level. Above this threshold, however, wave dissipation rapidly increases, so that the wave height spectrum is limited.

The improved model was first applied for fully-grown seas and then applied for a wide range of wind-wave conditions from laboratories to the open ocean. Kukulka and Hara (2008a,b) investigated the effect of air flow separation due to breaking waves on the air-sea momentum flux and concluded that the contribution of breaking waves is increasingly important for younger seas under higher wind speeds. However, the precise effects of surface breaking waves on the drag coefficient are still under investigation and are not yet explicitly calculated in our model. Since the effects of surface breaking waves and sea sprays on the drag coefficient are still uncertain, we instead introduced two purely empirical parameterizations of the drag coefficient based on the recent observations, as shown in Fig. 2. These new formulas are now being tested in the HWRF model.

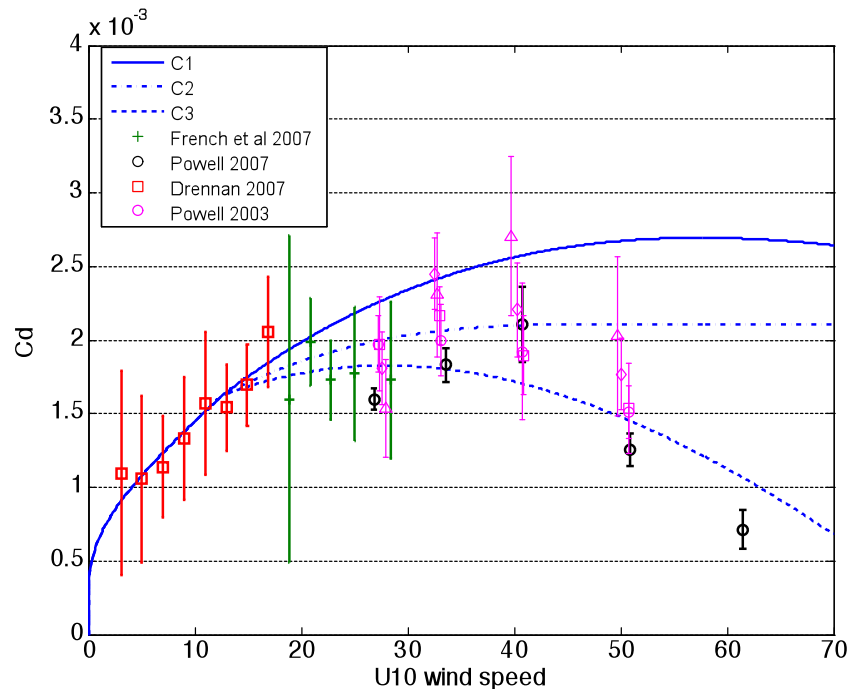


Figure 2. Three sea state independent drag coefficient formulae (C1: parameterization implemented into the operational HWRF and GFDL model; C2: proposed drag formula to saturate at high winds, C3: proposed drag formula to decrease at high wind) are compared with previous observations (symbols with error bars). Different symbols of Powell (2003) indicate estimates from different wind profile ranges.

b) Improving momentum flux parameterization in WW3 for hurricane conditions

It has been known that the WAVEWATCH III (WW3) wave model overestimates the significant wave height under very high wind conditions in strong hurricanes (Tolman et

al., 2005; Chao et al., 2005). Moon et al. (2008) suggested that one of the reasons for the overestimation of the significant wave height is due to overestimation of the drag coefficient in high wind conditions. In preparation for coupling of WW3 with HWRF, we have implemented the Moon et al. (2007) drag coefficient formulation into WW3. The effect of wave-current interaction in WW3 was also introduced and investigated under a tropical cyclone wind forcing (Fan et al. 2009a). The model results were compared with field observations of the surface wave spectra from a scanning radar altimeter, NDBC data and satellite altimeter measurements in Hurricane Ivan (2004) (Fig. 3). The results suggest that WW3 with the original drag coefficient parameterization tends to overestimate the significant wave height and the dominant wave length, and it produces a wave spectrum that is higher in wave energy and narrower in directional spreading. When an improved drag parameterization is introduced and the wave-current interaction is included, the model yields an improved forecast of significant wave height and wave spectral energy, but it underestimates the dominant wave length (Figs. 4 and 5).

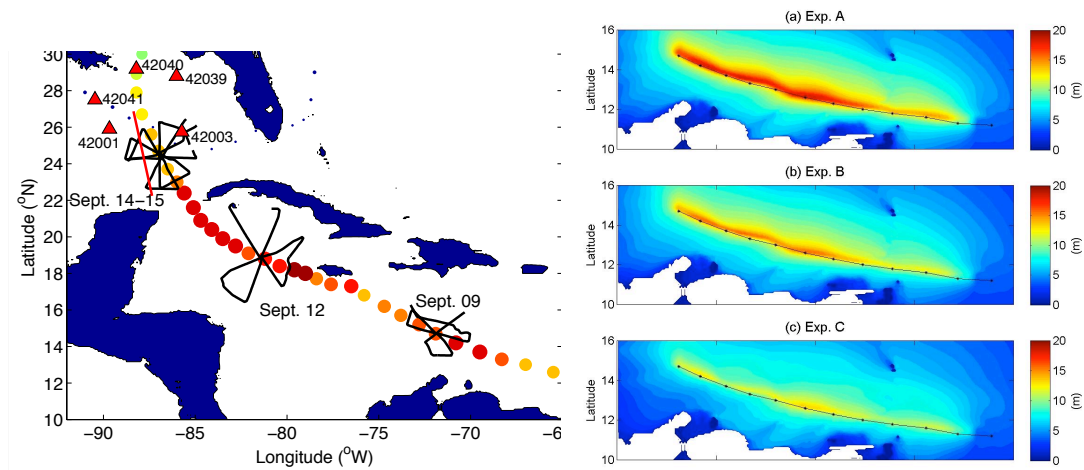


Figure 3. Left: Hurricane Ivan track from Sept. 6 0:00 UTC to Sept. 10 12:00 UTC. The color and size of the circle represent the maximum wind speed. Black lines represent the flight tracks during the SRA measurements. Right: Swath of maximum significant wave heights produced by WW3 using the original WW3 parameterization (Exp. A), the new parameterization (Exp. B), and the new parameterization with the wave-current interaction (Exp. C).

When a hurricane moves over mesoscale ocean features (warm- and cold-core rings, Loop Current), the current response can be significantly modulated by the non-linear interaction of the storm-induced and pre-existing strong currents in the mixed layer. We investigated the role of pre-existent currents due to mesoscale ocean features on wave predictions. Hurricane Ivan in 2004 crossed the Loop Current (LC) and a warm-core ring (WCR) in the Gulf of Mexico. Fortunately, during that time, detailed SRA wave spectra measurements were collected by NASA through a joint effort between the NASA/Goddard Space Flight Center and NOAA/HRD. These observations were used to investigate whether inclusion of the effect of pre-existent currents may improve the wave predictions using WW3.

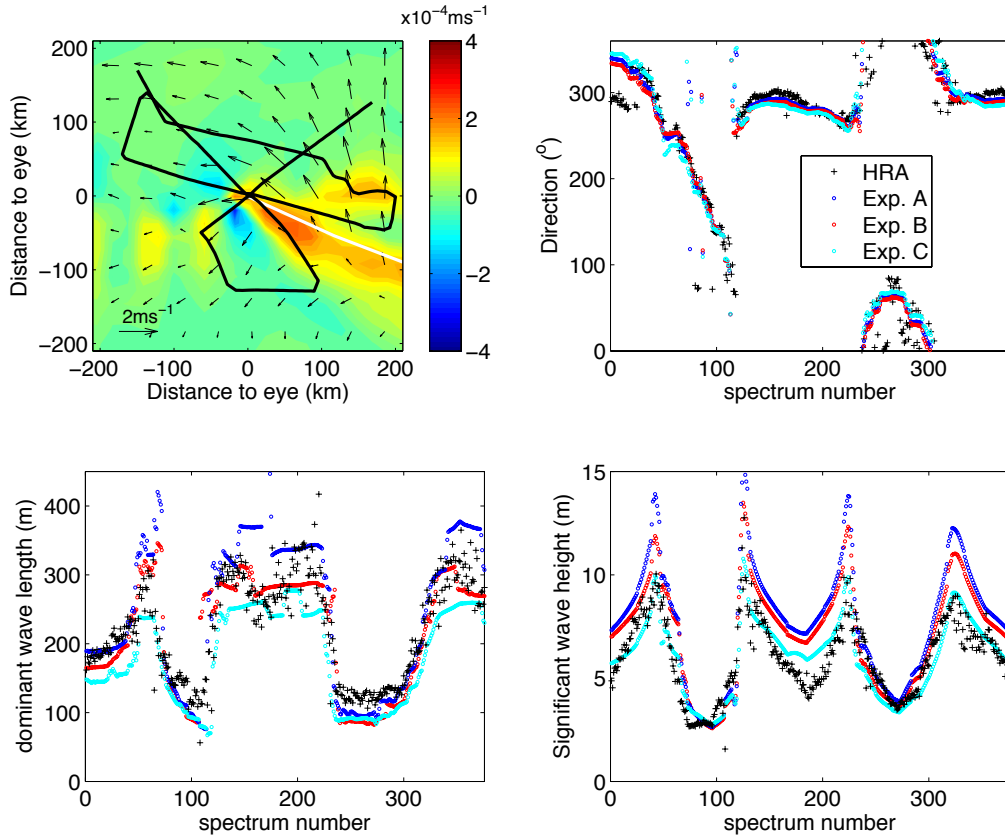


Figure 4. Upper left: WW3 wave field divergence in the run with the new flux parameterization and wave-current interaction at Sept. 9 18:00UTC. The color scale indicates significant wave height in meters; arrow length represents mean wave length, and arrow direction shows mean wave direction. Upper right, bottom right, and bottom left: wave direction, dominant wave length, and significant wave height, respectively.

We used the Colorado Center for Astrodynamic Research (CCAR) altimetry map on September 12, 2004 (Fig. 6a) to identify the position and structure of the LC and the WCR in the Gulf of Mexico. The feature-based modeling procedure of Yablonsky and Ginis (2008) was used to assimilate the altimetry observations into the ocean model (Fig. 6b). This ocean initialization procedure is the same as the one used in the operational HWRF and GFDL coupled models.

To investigate the effect of pre-existent currents, we compare two wave model simulations with and without the LC and WCR. Fig. 7c shows significant wave height (H_s) comparison between the two simulations along the September 14th – 15th flight. The SRA measurements are also shown for reference. The H_s difference between the two experiments is clearly seen along some of the flight sections. Let us examine two such periods highlighted by the gray areas in Fig. 7c. At 21:00 UTC on September 14, H_s is significantly larger with the LC initialization. The spatial snapshot of the H_s difference with and without the LC initialization is shown at the corresponding time in Fig. 7a. Fig. 6c shows the spatial distribution of the ocean temperature and current field at 70 m depth. At this time, the aircraft is over the edge of the LC, where a strong northward current is

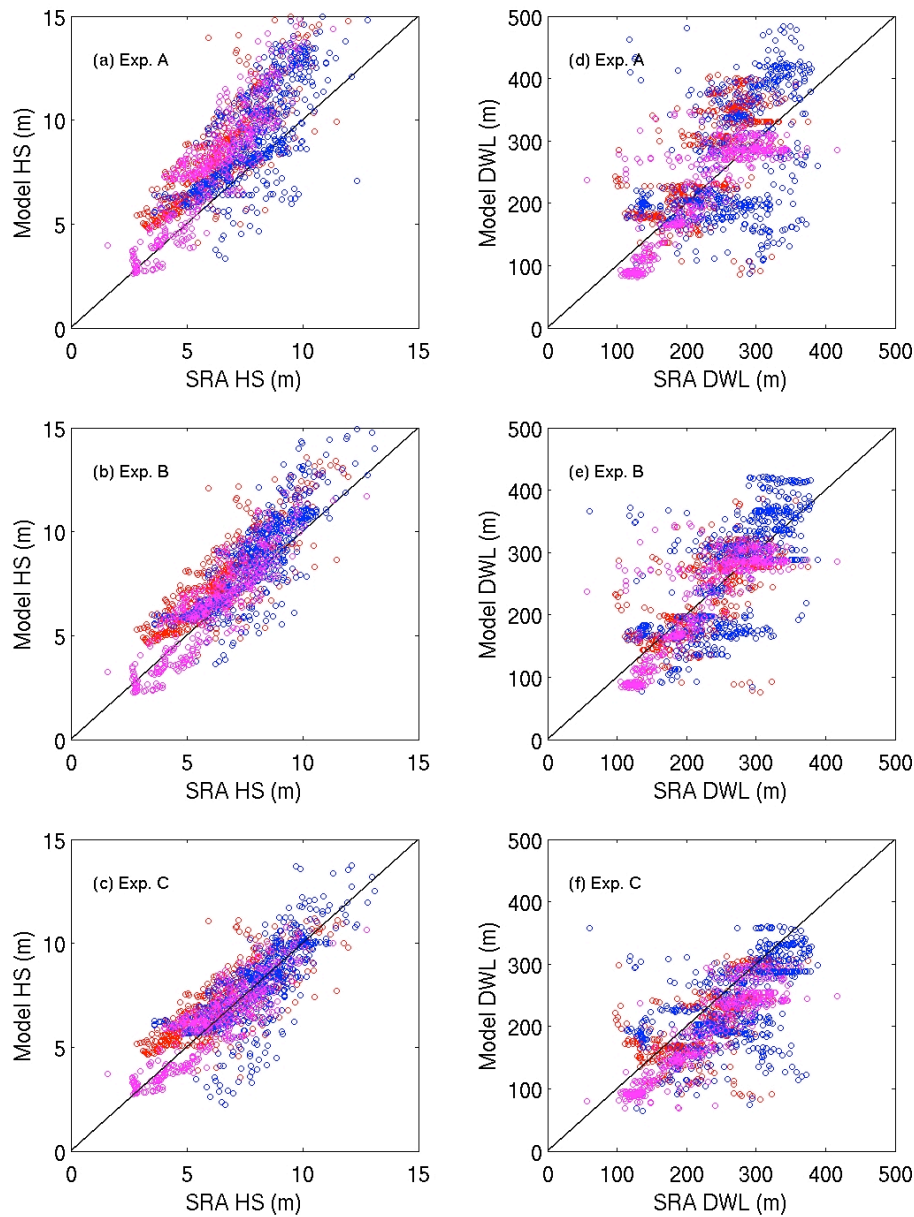


Figure 5. Model significant wave height (H_s) vs. SRA measurements (left panels); and model dominant wave length (DWL) vs. SRA measurements (right panels) for (d) Exp. A with original WW3 drag coefficient, (e) Exp. B with new drag coefficient based on the coupled wind wave model, and (f) Exp. C with the new drag coefficient and with the effect of ocean currents. The magenta, red, and blue circles correspond to the calculation period of September 9, 12 and 14-15.

added due to the LC initialization (Fig. 8a). The wave field at the same time (Fig. 8b) indicates that the dominant waves are propagating southward at this location. If we consider the evolution history of these dominant waves (along the pink arrows in Figs. 8a and 8b), it is evident that a strong opposing current persisted (i.e., the packet propagation was slower) throughout the wave evolution, such that the overall wave spectrum was enhanced. This wave spectrum enhancement explains why the predicted H_s at this location is increased when the Loop Current initialization is included.

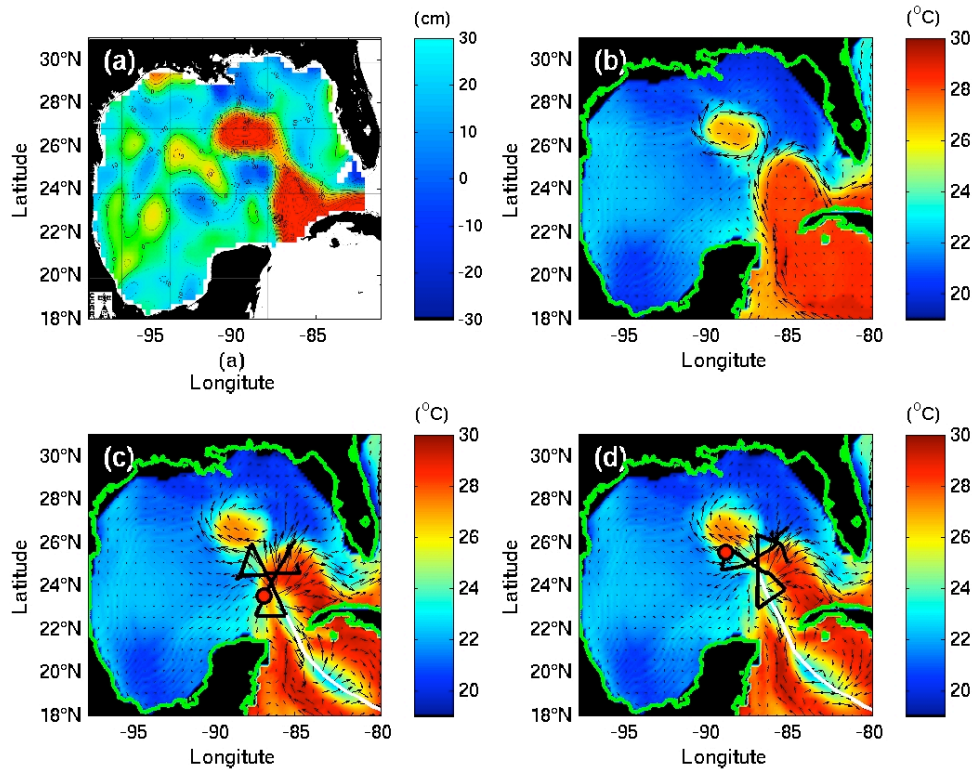


Figure 6. Satellite altimetry map in the Gulf of Mexico on September 12, 2004 (a), and ocean temperature at 70 m depth with current vectors at $L/4\pi$ depth in the ocean model at 12 UTC on September 12 (b), 21 UTC on September 14 (c), and 2:40 UTC on September 15 (d). On figure (c) and (d), the black line is flight track, the white line is hurricane track, the red dot shows the location of the SRA measurements at this time.

At 02:40 UTC on September 15, the predicted H_s is significantly smaller with the Loop Current initialization (Fig. 7c). Fig. 6d shows that the flight is passing through the southern edge of the warm core ring at this time. Due to the initialization of the warm core ring, a strong westward current is added at that location (Fig. 8c). The wave field at the same time (Fig. 8d) shows that the dominant waves are propagating westward. The evolution history of these dominant waves (along the pink arrows in Figs. 8c and 8d) is such that a strong positive (aligned) current accelerated the wave packet propagation and reduced the spectral level throughout the wave evolution.

These two examples clearly demonstrate that strong currents due to pre-existing mesoscale oceanic features may significantly modify the wave field prediction, mainly because such currents accelerate or decelerate the wave propagation.

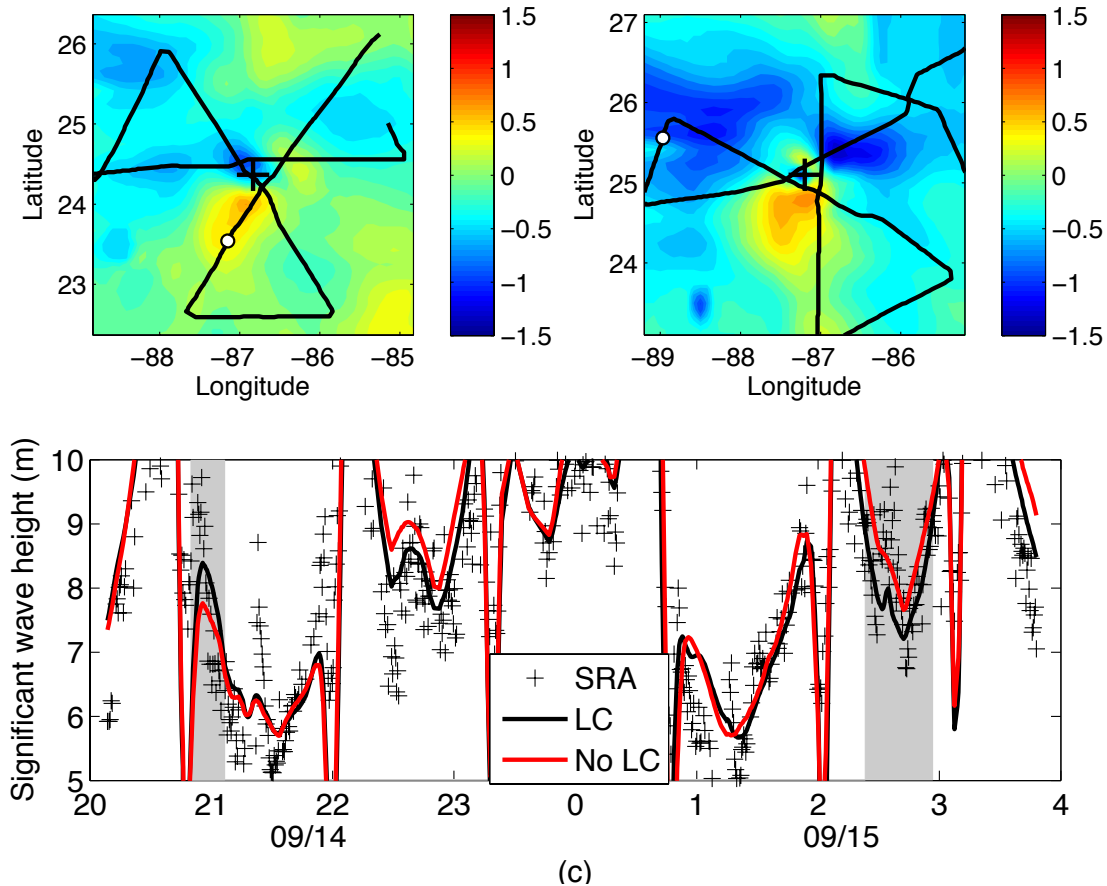


Figure 7. WW3 significant wave height (H_s) in the experiment with Loop Current initialization in the ocean model minus the H_s without Loop Current initialization at (a) 21 UTC on September 14, and (b) 2:40 UTC on September 15. (c) H_s with Loop Current (black line) and without Loop Current (red line) initialization in the ocean model compared with SRA observations (black cross).

c) Momentum flux budget at air-sea interface during hurricane-ocean interaction

In the present operational HWRF coupled hurricane model, momentum and kinetic energy fluxes into ocean currents are set to be exactly equal to the fluxes from air, neglecting their dependence on the sea state. However, under hurricane conditions the surface wave field is complex and fast varying in space and time and may significantly affect the fluxes at the air-sea interface. We performed numerical experiments under different idealized TC wind fields using a wind-wave coupled model and momentum flux budget equations (Fan et al. 2009c). The model results indicate that spatial and temporal variations of the TC-induced surface waves play an important role in reducing the kinetic energy and momentum fluxes into subsurface currents, mostly in the rear-right quadrant

of the TC. For a TC with maximum wind speed of 45 ms^{-1} , the reduction of the momentum flux can be as much as 10% in the vicinity of the radius of maximum wind (Fig. 9). These results suggest that it is important to explicitly resolve the effect of surface waves for accurate estimations of the momentum and kinetic energy fluxes at the air-sea interface in hurricanes.

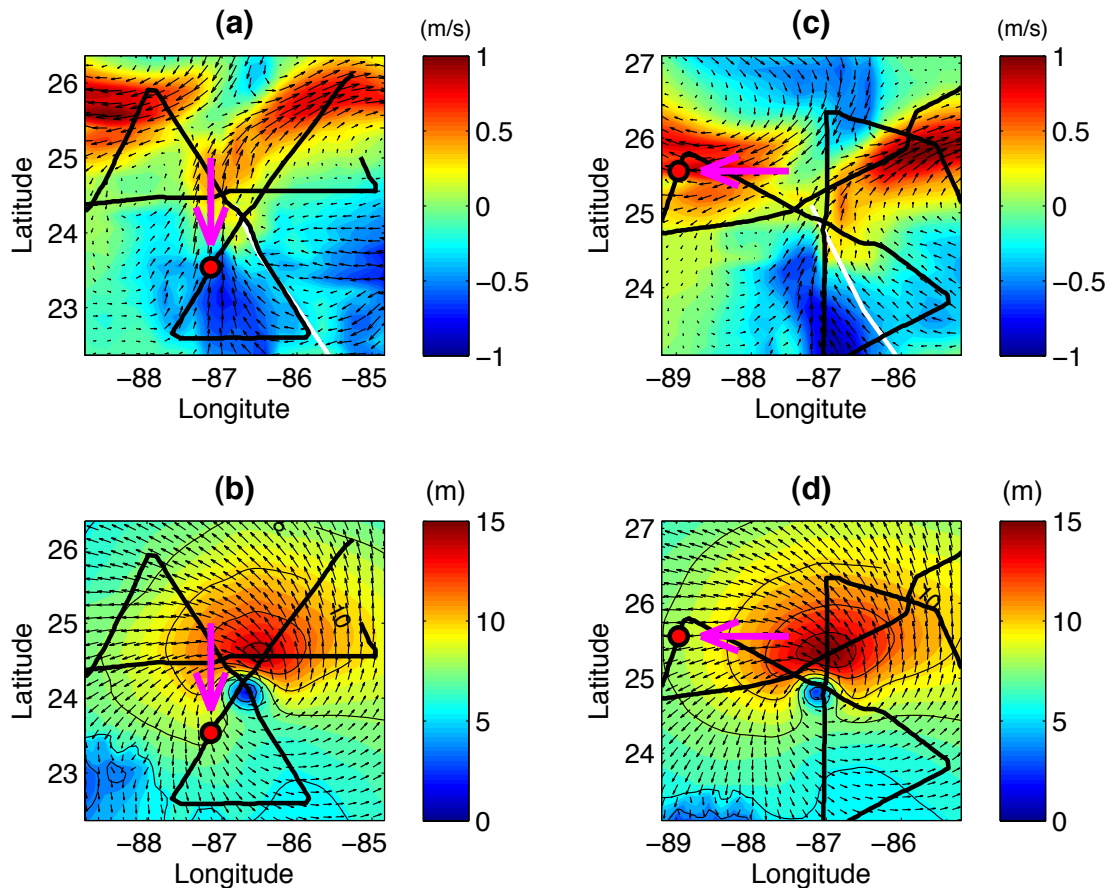


Figure 8. (a) Ocean current difference between the experiments with and without the Loop Current initialization at 21:00 UTC on September 14. (b) Significant wave height (H_s) in color and dominant wave length and direction in black arrows at 21:00 UTC on September 14. (c) Ocean current difference between the experiments with and without the Loop Current initialization at 2:40 UTC on September 15. (d) Significant wave height (H_s) in color and dominant wave length and direction in black arrows at 2:40 UTC on September 15. The black line shows the flight track and the red dots show the location of the flight at the time that the current and wave field are shown. The pink arrow shows the wave propagation path.

We investigated the effects of air-sea momentum budget and wind-wave-current interaction on the ocean response through a set of numerical experiments (Fan et al. 2009b). The results show that the temporal and spatial variations in the current field reduce the momentum flux into the currents, primarily in the rear-right quadrant of the hurricane. The reduction of the momentum flux into the ocean consequently reduces the magnitude of the subsurface current and sea surface temperature cooling to the right of the hurricane track and the rate of upwelling/downwelling in the thermocline (Fig. 10).

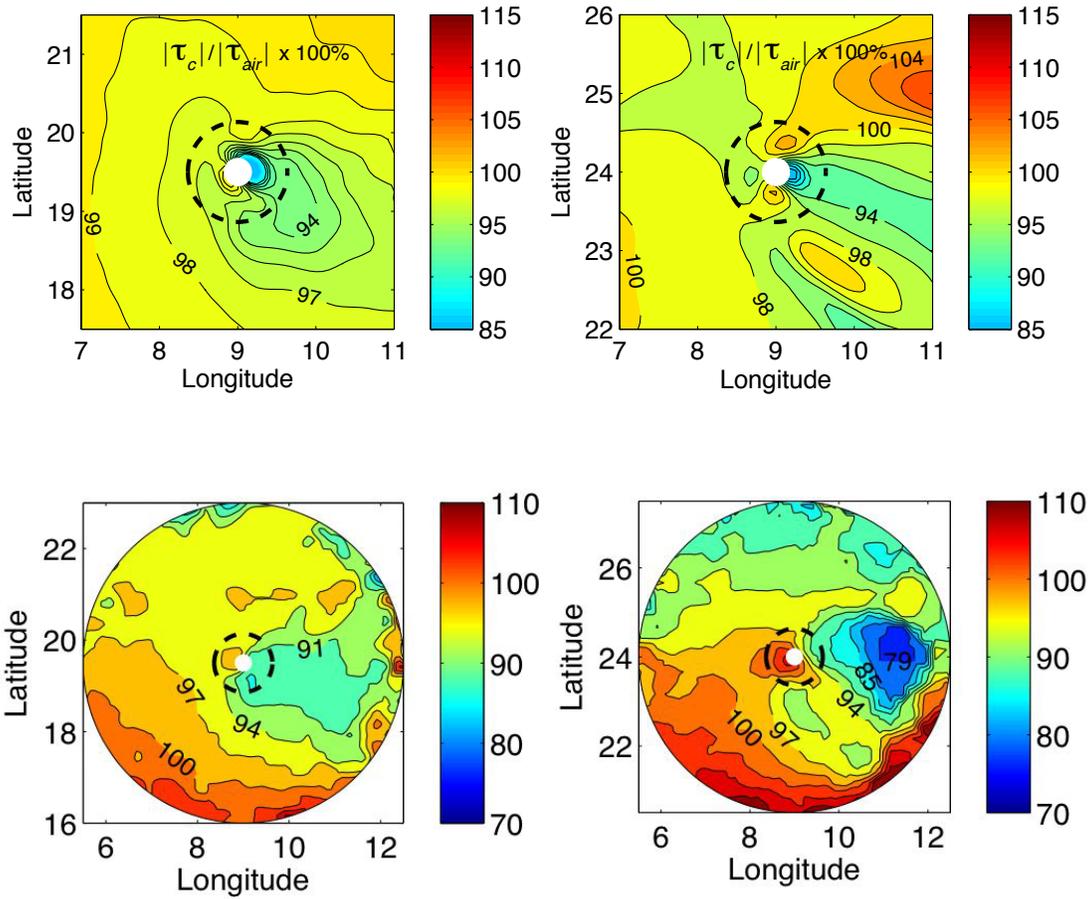


Figure 9. Percentage of momentum (top) and kinetic energy (bottom) fluxes into subsurface currents relative to air input produced by the idealized moving tropical cyclone with the translation speed of 5ms^{-1} (left) and 10ms^{-1} (right). The dashed circle and white dot represent the radius of maximum wind and the center of the tropical cyclone, respectively.

II. Improving air-sea momentum and heat flux parameterization in the HWRF model

a) Air-sea interface module (ASIM)

We developed and transitioned to NCEP/EMC a new air-sea interface module (ASIM), which is currently being coupled with the HWRF model. Since the air-sea fluxes depend on surface wave-related processes and are highly variable in space and time, the ASIM module includes parameterizations of the coupled wind-wave-current physical processes as follows: 1) in the atmospheric model, the parameterizations of the air-sea heat and momentum fluxes explicitly include the sea state dependence and ocean currents; 2) the wave model is forced by the sea-state dependent momentum flux and includes the ocean current effects; 3) the ocean model is forced by the sea-state dependent momentum flux that accounts for the air-sea flux budget.

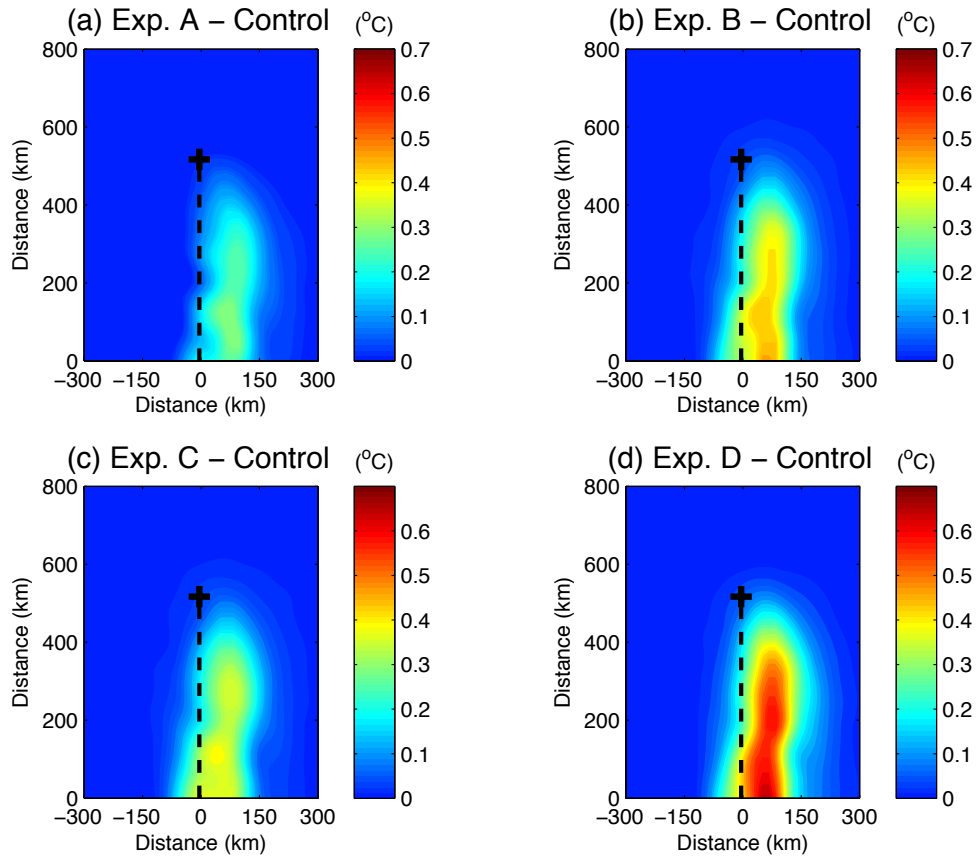


Figure 10. SST anomaly differences between experiments. (a) effect of air-sea flux budget, (b) effects of current on wind and waves, (c) effect of current on wind only, (d) all effects. The colors scale represents temperature in degrees ($^{\circ}\text{C}$) with positive/negative denote decrease/increase of SST cooling. The black cross and dashed line on the panels indicate the center and track of the hurricane.

The new coupled modeling framework is shown in Figure 11. The ASIM consists of 1) the coupled wind-wave (CWW) boundary layer model of Moon et al. (2004a,b) (module “MFLUX” in Fig. 11 and 2) the air-sea energy and momentum flux budget model of Fan et al. (2009a,b, c) (modules “MFBudget” and “WFlux” in Fig. 11). During this project, the ASIM has been coupled with the NOAA/ESRL sea spray model (sub-module “sea spray model” in Fig. 11) and augmented with the new parameterization of breaking waves on momentum and energy fluxes based on the theoretical studies Kukulka and Hara (2008a,b).

The ASIM will be imbedded into the HWRF hurricane-wave-ocean coupled model and will calculate all of the flux boundary conditions for the atmospheric, wave, and ocean models. Our EMC colleagues have modified the atmosphere-ocean coupler in HWRF to include explicit coupling with the WAVEWATCH III wave model. We have been working with the EMC group to assist in the testing of the atmosphere-wave-ocean coupler and the URI ASIM module.

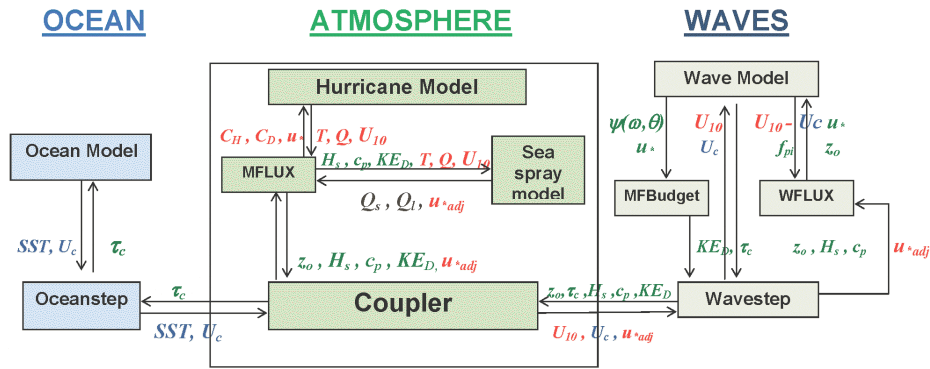


Figure 11. A schematic diagram of the coupled wind-wave-current modeling system and the air-sea interface module (ASIM) represented by the following components: MFLUX, Sea spray model, MFBudget, and WFLUX. The arrows indicate the prognostic variables that are passed between the model components.

Here we briefly describe two important components of the ASIM: MFBudget and Sea spray (Fig. 11). In modeling the ocean response to tropical cyclones, the momentum flux into subsurface currents (τ_c) is the most critical parameter. Research and operational coupled atmosphere-ocean models usually assume that τ_c is identical to the momentum flux from wind (wind stress) τ_{air} , that is, no net momentum is gained (or lost) by surface waves. This assumption, however, is invalid when the surface wave field is growing or decaying. With inclusion of wave coupling, the momentum gain/loss by surface waves can be explicitly calculated, as shown in Fig. 12. The air-sea momentum flux budget model MFBudget is used to estimate the difference between the momentum flux from air and the flux to subsurface currents.

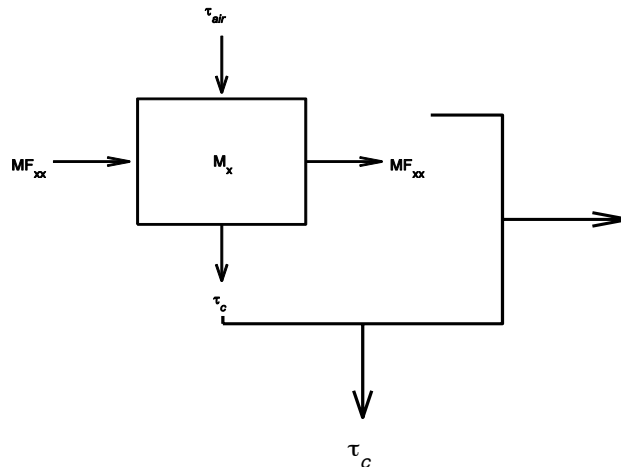


Figure 12. Air-sea momentum budget diagram at the air-sea interface (MFBudget module in Fig. 11). The details of flux calculations are discussed in Fan et al. (2009c).

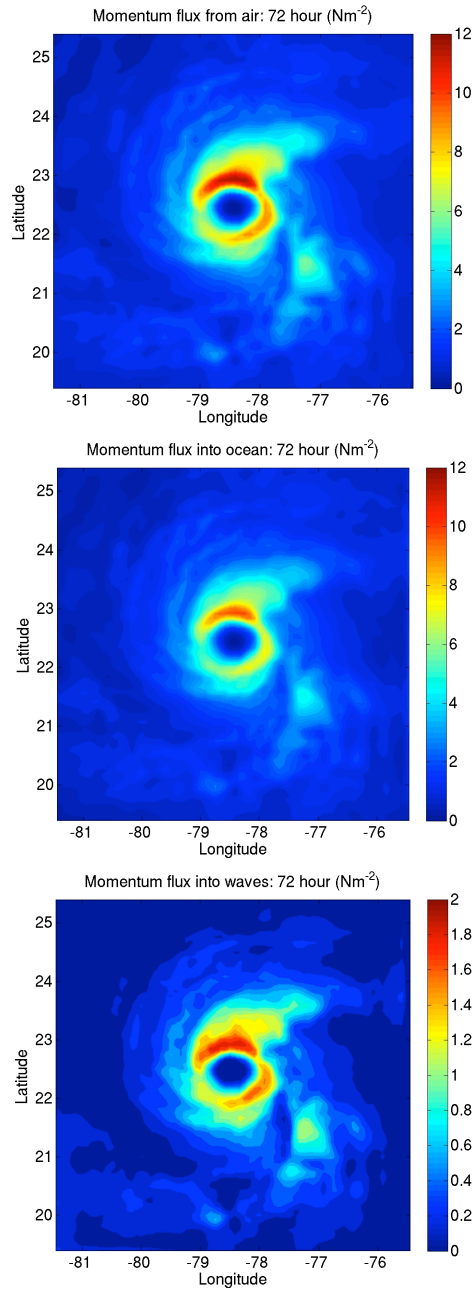


Figure 13. Momentum flux from air (upper panel), into the ocean (middle panel) and the difference (low panel) in an idealized, fully-coupled hurricane-wave-ocean model. The storm in this experiment was propagating towards the northwest.

We investigated the effect of surface gravity waves on the air-sea momentum flux budget under TC wind conditions in a set of numerical experiments using an idealized TC with different translation speeds, intensities, and structure. The results suggest that surface waves may significantly reduce the momentum flux into currents relative to the wind stress. Figure 13 compares the momentum flux from the air (wind stress) and the momentum flux into the ocean in an idealized, fully-coupled hurricane model

experiment. The differences between these fluxes reach more than 2 N/m^2 , primarily to the right and behind the storm center.

One of the novel features implemented in ASIM is the method of coupling between breaking waves and the NOAA/ESRL sea spray generation model. In the present NOAA/ESRL sea-spray model, the source function is parameterized in terms of energy lost to the wave breaking process, EF_c , which is simply related to the wind speed. The effective droplet source height h is related to the significant wave height. Within the framework of ASIM, the total energy lost to breaking (EF_c) is accurately estimated by explicitly accounting for the sea state dependence and the air-sea flux budget (Fan et al., 2009c). The source height h is determined not from the significant wave height but from the input wave age (wave age of the wind-forced part of the spectrum) and the wind stress (Fan et al., 2009a,b). This modification is important under tropical cyclones because the dominant scale of breaking waves is related to the scale of the actively wind-forced waves – not related to the scale of swell generated elsewhere.

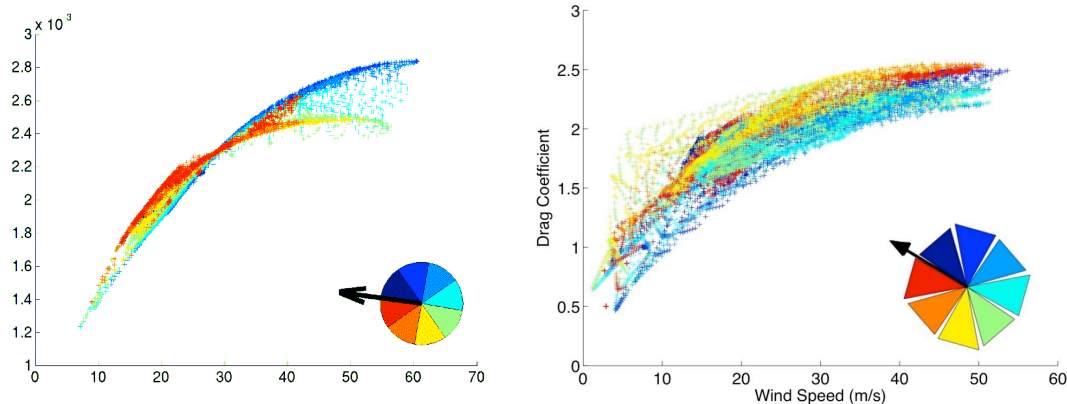


Figure 14. Drag coefficient, C_d , in the experiment with the GFDL hurricane model when only the effect of wind-wave coupling is included (left) and in the experiment with the fully coupled wind-wave-current GFDL hurricane model (right).

The URI ASIM code has been transferred to the NOAA/ESRL group for imbedding the ESRL sea spray model. Once this task is completed, we will proceed with testing and evaluating the effect of sea spray on the air-sea fluxes within a framework of a fully-coupled hurricane-wave-ocean system.

b) Testing of ASIM in the GFDL hurricane model

While the fully coupled HWRF wind-wave-current model is being developed, we implemented the ASIM into the experimental version of the GFDL-WAVEWATCH III-POM coupled system and conducted idealized and real-case simulations. One of the most important results obtained in these experiments is a significant effect of the wind-wave-ocean coupling on the spatial distribution of the drag coefficient (C_d), as illustrated in Fig. 14. The drag coefficient scatter plot show significant differences between the experiments with and without the effect of wind-wave-current interaction. In the

experiment that accounts only for the wind-wave interaction, the maximum C_d is found in the front right quadrant, while in the experiment with the full wind-wave-current interaction, the largest C_d is found in the front left quadrant. This result suggests that the strong hurricane-generated current to the right of the storm track tends to reduce the drag coefficient.

We found that the changes in the spatial distributions of the drag coefficient can affect the surface wind structure and the hurricane track forecast. Figure 15 shows the predicted surface wind and C_d fields in Hurricane Rita in the operational and fully coupled GFDL models (Initial time: Sept. 20, 2005 12Z) that clearly illustrate the importance of the wind-wave-ocean coupling on the hurricane wind structure. These changes in the hurricane winds led to improved track forecasts as shown in two test simulations of Hurricane Rita (Initial times: Sept. 19 00 Z and Sept. 20 12Z) using the operational and the fully coupled GFDL hurricane models (Fig. 16).

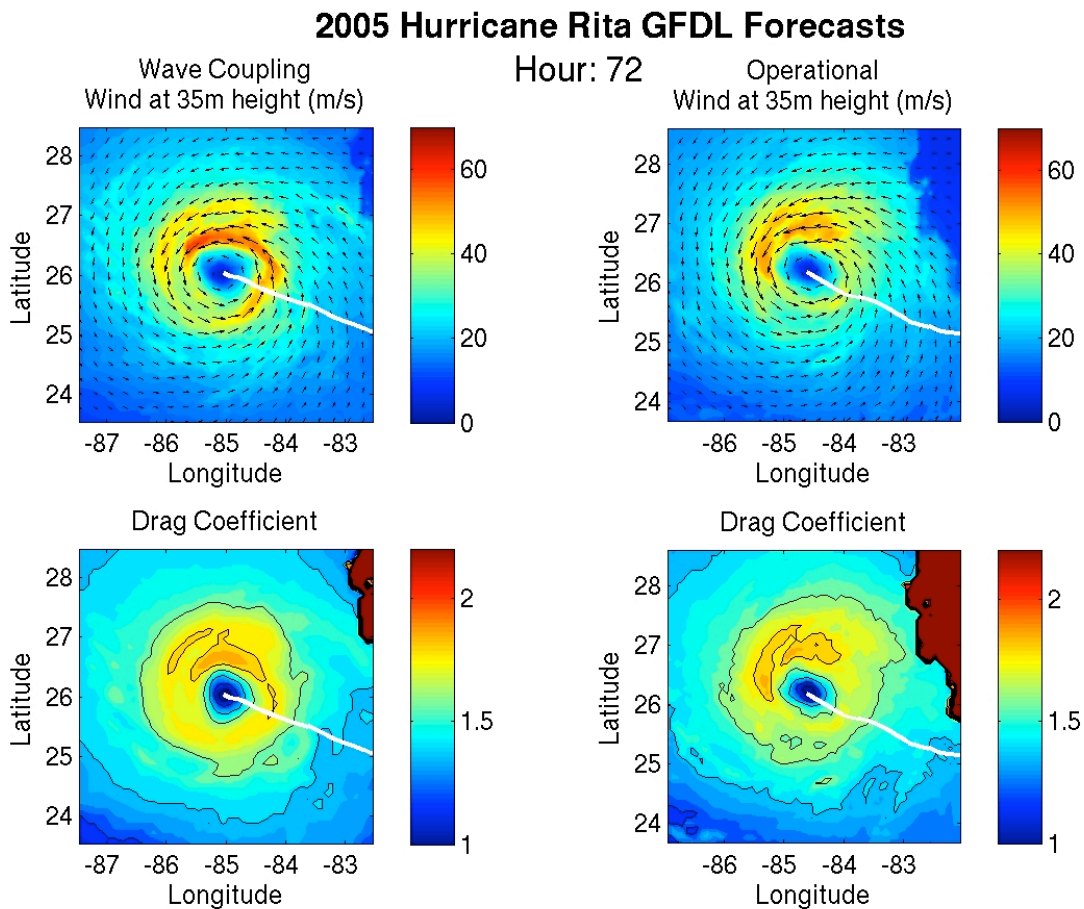


Figure 15. Drag coefficient and 35m wind in the two Hurricane Rita (2005) simulations (Initial time Sept. 20, 2005 12Z) in the fully coupled (left) and operational (right) GFDL hurricane models.

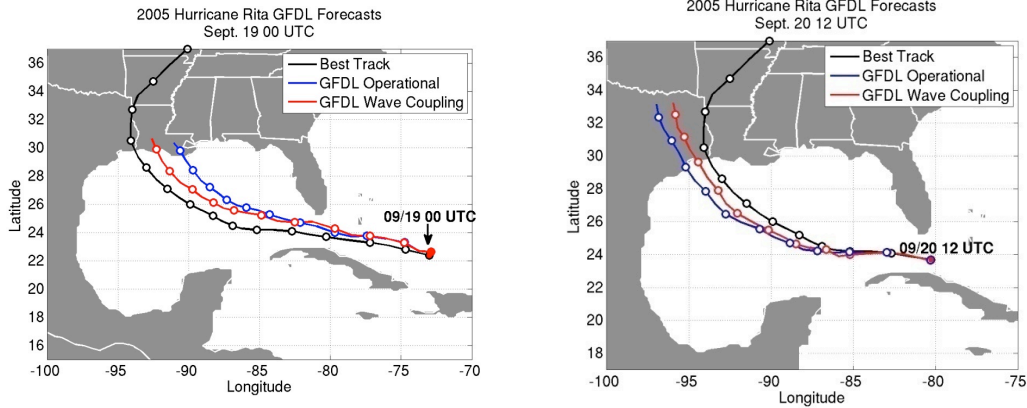


Figure 16. Track forecasts in the test simulations of Hurricane Rita (Initial times: Sept. 19 00Z and Sept. 20 12Z) using the operational (blue) and the fully coupled (red) GFDL hurricane models.

III. Improving ocean initialization in the HWRF coupled system by implementing new methods for assimilating satellite and in-situ measurements.

Coupled hurricane-ocean forecast models require proper initialization of the ocean thermal structure. Yablonsky and Ginis (2008) have created a feature-based (F-B) ocean initialization procedure to account for spatial and temporal variability of mesoscale oceanic features in the Gulf of Mexico, including the Loop Current (LC), warm-core rings (WCRs) and cold-core rings (CCRs). Using this F-B procedure, near real-time maps of sea surface height and/or the 26°C isotherm depth, derived from satellite altimetry, can be used to adjust the position of the LC and insert WCRs and/or CCRs into the background climatological ocean temperature field prior to hurricane passage.

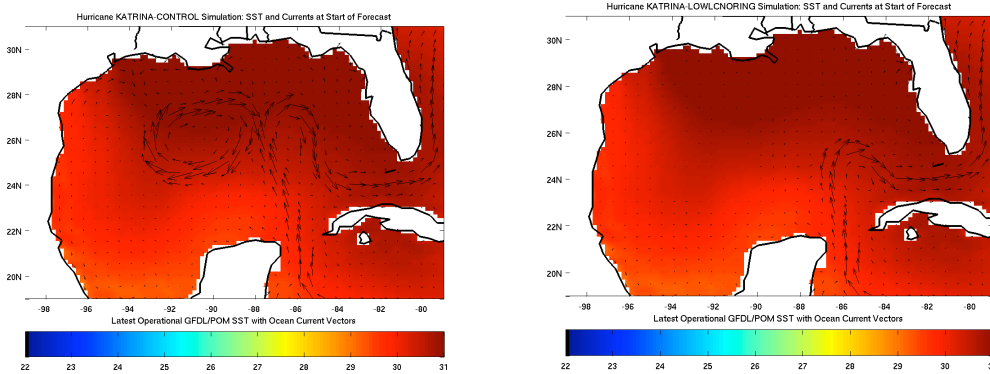


Figure 17. SST and surface currents for Hurricane Katrina coupled GFDL model forecasts with the Loop Current and a warm core ring initialized based on altimetry to represent the actual location as of 26 August 2005 (left panel) and a modified Hurricane Katrina coupled GFDL model forecast in which the Loop Current is initialized in its climatological position, and no warm core ring is assimilated (right panel).

The 2007 version of the feature-modeling ocean initialization procedure used operationally HWRF model had the following limitations with regards to assimilating features in the Gulf of Mexico: (1) Only one WCR could be assimilated, not multiple rings, (2) CCRs could not be assimilated, (3) the LC had to connect to an adjacent WCR if the WCR was in close proximity to the LC (in order to suppress unphysical interaction between these two features), and (4) *in situ* ocean temperature profiles could not be used to define the center temperature profile of the LC and/or rings. During the 2007 Atlantic hurricane season, satellite altimetry was used by the Tropical Prediction Center (TPC) to generate 26°C-isotherm maps (and oceanic heat content maps) for the Gulf of Mexico in real-time. Subsequently, TPC staff assimilated these 26°C-isotherm maps into the feature-modeling ocean initialization procedure by subjectively defining LC and, when applicable, WCR perimeter points.

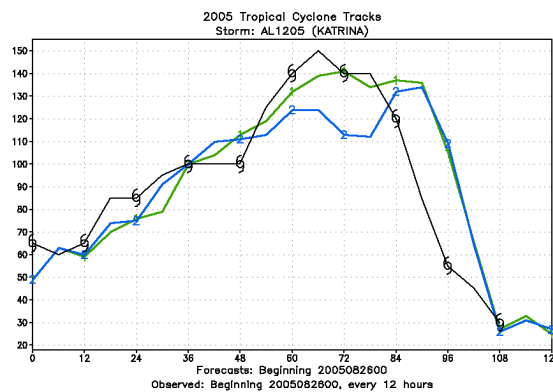


Figure 18. Hurricane Katrina maximum wind speed (kt) for CTRL (green line; “1” symbols), CLIM (blue line; “2” symbols), and observations (black line; hurricane symbols).

For the 2008 Atlantic hurricane season, a new version of the feature-modeling ocean initialization procedure (Yablonsky and Ginis, 2008) was transitioned to the operational HWRF coupled hurricane-ocean model. The version was designed to more accurately initialize the LC and WCRs/CCRs using satellite altimetry and *in situ* data in the Gulf of Mexico. We worked with TPC staff to implement these changes before the start of the 2008 hurricane season. It is worthwhile to note that the new version can also assimilate real-time *in situ* data such as AXBT profiles, as discussed in Yablonsky and Ginis (2008).

To evaluate the impact of assimilating mesoscale oceanic features on both the SST cooling under the storm and the subsequent intensity change of the storm coupled hurricane-ocean model sensitivity experiments for selected hurricanes were run with and without altimeter data assimilation. Simulations of Hurricane Katrina (2005) are shown in Fig. 17 and Fig. 18. In the CTRL case, the Loop Current and a WCR are assimilated using altimetry to accurately represent these features (Fig. 17a). In the CLIM case, the Loop Current is initialized instead in its climatological position, and no WCR is assimilated (Fig. 17b). The presence of the Loop Current and WCR reduced the SST cooling along the hurricane track in the CTRL case (not shown) and allowed the storm to

become more intense (Fig. 18). In fact the CTRL case forecasts the intensity of the actual storm much better than the CLIM case does.

We also investigated the impact of WCRs on hurricane-induced surface cooling. In recent years, it has become widely accepted that the upper oceanic heat content (OHC) in advance of a hurricane is generally superior to pre-storm sea surface temperature (SST) for indicating favorable regions for hurricane intensification and maintenance. The OHC is important because a hurricane's surface winds mix the upper ocean and entrain cooler water into the oceanic mixed layer from below, subsequently cooling the sea surface in the region providing heat energy to the storm. For a given initial SST, increased OHC typically decreases the wind-induced sea surface cooling, and a warm ocean eddy has a higher OHC than its surroundings, so the argument is often made that conditions become more favorable for a hurricane to intensify when the storm's core encounters a WCR. When considering hurricane intensity, one often neglect aspect of a WCR is the anticyclonic circulation in the eddy that exists due to the geostrophic adjustment of the density and velocity fields.

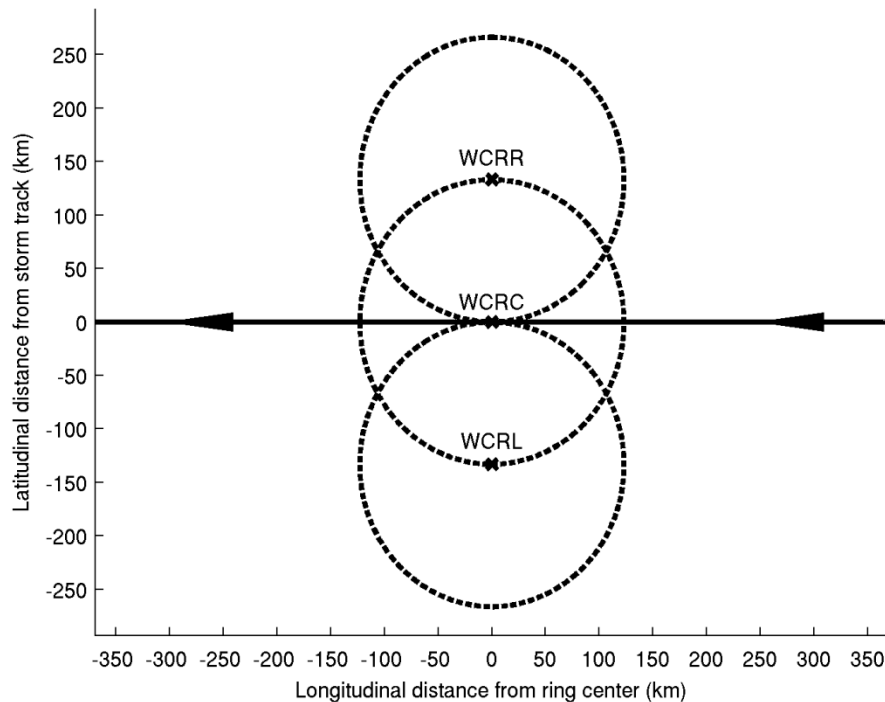


Figure 19. Schematic indicating the WCR position when located in the center of the storm track (WCRC), to the south (i.e. left) of the storm track (WCRL), and to the north (i.e. right) of the storm track (WCRR). Storm track and direction are indicated by the horizontal line with embedded, westward-pointing arrows.

In a series of idealized numerical experiments, a WCR is assimilated into the otherwise horizontally-homogeneous ocean using the feature-based methodology of Yablonsky and Ginis (2008). This WCR is nearly circular in shape, with a radius of 1.2° (i.e. 133 km along the north-south axis and 123 km along the east-west axis), which is typical of

WCRs in the Gulf of Mexico. The hurricane wind stress field translates due westward towards and then past a WCR centered at 85.7°W. Experiments are performed with the WCR located in the center of the storm track (WCRC), to the south (i.e. left) of the storm track (WCRL), and to the north (i.e. right) of the storm track (WCRR) (Fig. 19). The results are compared with the control experiment (CTRL) in which there is no WCR specified.

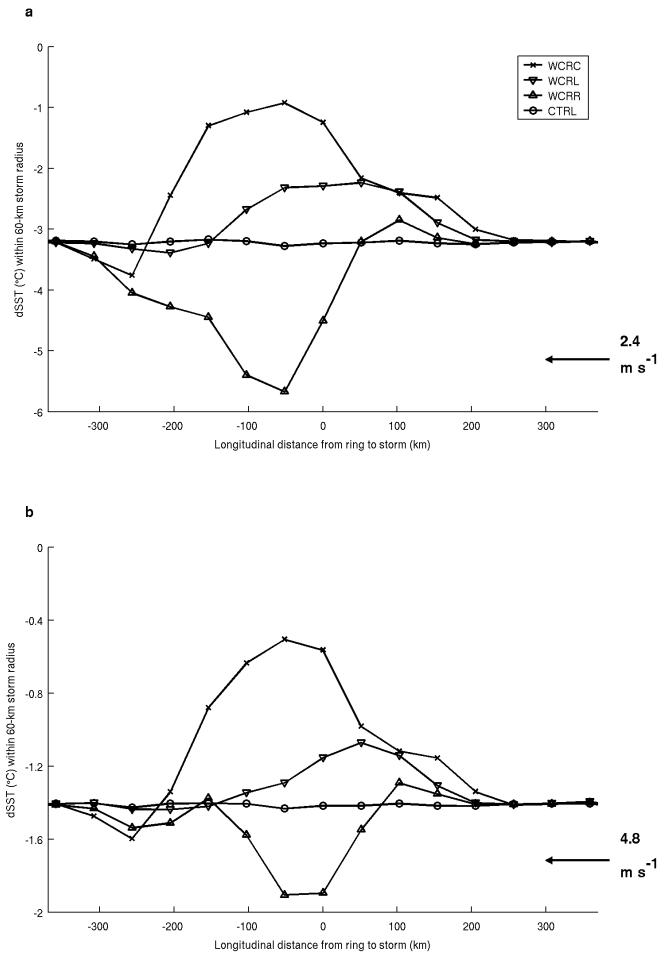


Figure 20. Average SST cooling within a 60-km radius of the storm center ($dSST-60$) for the experiments with translation speeds of 2.4 m s^{-1} (a) and 4.8 m s^{-1} . Each panel includes WCRC (“x”), WCRL (downward triangle), WCRR (upward triangle), and CTRL (“o”) experiments.

Since the goal of this investigation is to quantify the magnitude of SST cooling only within the region providing most of the heat energy to the storm, the average SST cooling is calculated within a 60-km radius around the storm center (hereafter $dSST-60$) while the storm-induced cooling is being influenced by the WCR (when present). In the WCRC and WCRL experiments, the magnitude of $dSST-60$ generally decreases as the storm approaches the WCR and then increases towards its original value as the storm passes the WCR. This trend is consistent with the purely thermodynamic view of a WCR, whereby the deeper mixed layer within the WCR restricts the ability of the storm to entrain a

significant quantity of cooler water into the upper oceanic mixed layer via shear-induced mixing. The most significant and perhaps unexpected result occurs in the WCRR experiment. The magnitude of the dSST-60 in this experiment increases dramatically as the storm passes the WCR (Fig. 20). It turns out that this increase in the magnitude of the dSST-60 is caused by the WCR's anticyclonic circulation, which advects the storm's cold wake horizontally in the direction of the storm track, thereby increasing the SST cooling underneath the storm core. This effect is clearly seen in Fig. 21, which shows the SST and current vector difference field between WCRR and CTRL when the storm center is ~ 50 km and ~ 250 -km past the WCR's center longitude.

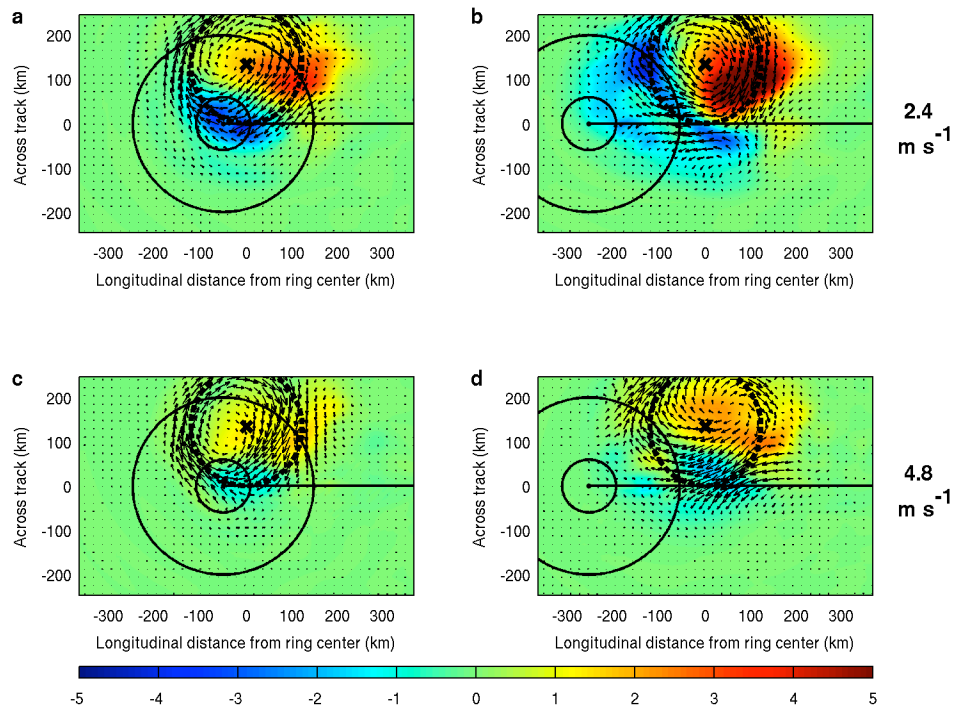


Figure 21. WCRR – CTRL SST ($^{\circ}$ C) and surface current vector difference field when storm center is ~ 50 km (a, c) and ~ 250 km (b, d) past the WCR's center longitude for 2.4 m/s, and 4.8 m/s experiments. Thin solid circles indicate 60-km and 200-km radii from the storm center; thick dashed circle indicates the WCR's perimeter.

References:

- Andreas, E. L., 2004: Spray stress revisited. *J. Phys. Oceanogr.*, **34**, 1429–1440.
- Black, P. G., and Coauthors, 2007: Air–sea exchange in hurricanes: Synthesis of observations from the Coupled Boundary Layer Air–Sea Transfer Experiment. *Bull. Amer. Meteor. Soc.*, **88**, 357–374.
- Chao, Y. Y., J.-H. G. M. Alves, and H. L. Tolman, 2005: An operational system for predicting hurricane-generated wind waves in the north Atlantic Ocean. *Wea. Forecasting*, **20**, 652–671.

- Drennan, W. M., J. Zhang, J. R. French, C. McCormick, P. G. Black, 2007: Turbulent fluxes in the hurricane boundary layer. Part II: Latent heat flux. *J. Atmos. Sci.*, **64**, 1103–1115.
- Fan, Y., I. Ginis, T. Hara, W. Wright, and E. Walsh, 2009a, Numerical simulations and observations of the surface wave fields under an extreme tropical cyclone. *J. Phys. Oceanogr.*, **39**, 2097–2116
- Fan, Y., I. Ginis, and T. Hara, 2009b, The effect of wind-wave-current interaction on air-sea momentum fluxes and ocean response in tropical cyclones. *J. Phys. Oceanogr.*, **39**, 1019–1034.
- Fan, Y., I. Ginis, and T. Hara, 2009c, Momentum flux budget across air-sea interface under uniform and tropical cyclones winds. *J. Phys. Oceanogr.*, in review.
- Kukulka, T., and H. Hara, 2008a. The effect of breaking waves on a coupled model of wind and ocean surface waves: I. Mature seas, *J. Phys. Oceanogr.*, **38**, 2145–2163.
- Kukulka, T., and H. Hara, 2008b. The effect of breaking waves on a coupled model of wind and ocean surface waves: II. Growing seas, *J. Phys. Oceanogr.*, **38**, 2164–2184.
- Moon, I.-J., I. Ginis, and T. Hara, 2004a: Effect of surface waves on Charnock coefficient under tropical cyclones, *Geophys. Res. Lett.*, **31**, L20302.
- Moon, I.-J., T. Hara, I. Ginis, S. E. Belcher, H. L. Tolman, 2004b: Effect of surface waves on air-sea momentum exchange. Part I: Effect of mature and growing seas, *J. Atmos. Sci.*, **61**, 2321–2333.
- Moon, I.-J., I. Ginis, and T. Hara, 2004c: Effect of surface waves on air-sea momentum exchange. Part II: Behavior of drag coefficient under tropical cyclones, *J. Atmos. Sci.*, **61**, 2334–2348.
- Moon, I.-J., I. Ginis, and T. Hara, 2008: Impact of the reduced drag coefficient on ocean wave modeling under hurricane conditions. *Mon. Wea. Rev.*, **136**, 1217–1223.
- Moon, I., I. Ginis, and T. Hara, B. Thomas, 2007: Physics-based parameterization of air-sea momentum flux at high wind speeds and its impact on hurricane intensity predictions. *Mon. Wea. Rev.* **135**, 2869–2878.
- Powell, M. D., P. J. Vickery, and T. A. Reinhold, 2003: Reduced drag coefficient for high wind speeds in tropical cyclones. *Nature*, **422**, 279–283.
- Powell, M. D, 2007: Drag coefficient distribution and wind speed dependence in tropical cyclones, JHT Final Report. April 2007.
- Tolman H., J. H. G. M. Alves, and Y. Y. Chao, 2005: Operational forecasting of wind-generated waves by Hurricane Isabel at NCEP. *Wea. Forecasting*, **20**, 544–557.
- Yablonsky, R. M., and I. Ginis, 2008: Improving the ocean initialization of coupled hurricane-ocean models using feature-based data assimilation. *Mon. Wea. Rev.*, **136**, 2592–2607.